THE SPECTRUM OF OPEN CONFINING STRINGS IN THE LARGE- N_c LIMIT

The 41st International Symposium on Lattice Field Theory ,Liverpool, UK 28 July - 3 August 2024.
Alireza Sharifian[†], Pedro Bicudo[†], and Andreas Athenodorou[‡].
[†]CeFEMA, Departamento de Física, Instituto Superior Técnico, Universidade de Lisboa, Portugal.
[‡]Computation-based Science and Technology Research Center, The Cyprus Institute, Cyprus.

ABSTRACT

We compute the spectra of open flux tubes formed between a static quark-antiquark pair for various gauge groups in the large-N_c limit, focusing on different symmetries. Specifically, we present spectra up to $N_c = 6$ and for eight different symmetries of the flux tube. In this study, we employed an anisotropic Wilson action, a large number of suitable operators, and solved the generalized eigenvalue problem (GEVP) to identify a significant number of excitations for different flux tube symmetries. The spectra are compared with the Nambu-Goto string model, revealing novel phenomena such as the presence of massive axions in the flux tube. We find that the mass of the axion in the open flux tube spectra sector is consistent with the mass obtained in the closed flux tube sector.

INTRODUCTION

1 Preamble

In confining gauge theories such as $SU(N_c)$ gluodynamics, the energy of a gauge field from color charges can be compressed into flux tubes, forming confining strings. Understanding the dynamics of the worldsheet of these strings is crucial for comprehending color confinement. Over the past decade, significant advancements have been made in understanding the effective string theoretical description of the *closed* flux tube [1, 2]. Notably, the dynamics of the world-sheet theory have been derived from lattice data in a model-independent manner. This analysis revealed the presence of several string-like states and a massive excitation known as the world-sheet axion. However, a similar investigation is lacking for the case of the *open* flux tube. In this work, we shed light on the large-N_c limit of the spectrum of open flux-tubes and the existence of axions in their worldsheet.

2 The Nambu-Goto string

The Nambu-Goto string model is defined by the action

$$S = -\sigma \int \mathrm{d}^2\Sigma, \tag{1}$$

where σ is the string tension and Σ is the surface of the worldsheet swept by the string. The energy of an open relativistic string with length R and fixed ends is obtained as

$$V(R) = \sqrt{\sigma^2 R^2 + 2\pi\sigma(N - (D-2)/24)}, \tag{2}$$

where N is the quantum number for string vibrations and D is the dimension of space time. This expression is known as the Arvis potential [3].

3 Quantum Numbers of the flux tube

There are three constants of motion whose eigenvalues are used to label the quantum state of the flux tube:

- z-component of angular momentum $\Lambda = 0, 1, 2, 3, \ldots$, they are typically denoted by greek letters Σ, Π, Δ, $\Phi, \ldots$, respectively
- Combination of the charge conjugation and spatial inversion with respect to the mid point of the charge axis operators $\mathcal{P}o\mathcal{C}$, its eigenvalues $\eta = 1, -1$, they are denoted by g, u, respectively.
- For $\Sigma(\Lambda = 0)$, reflection with respect to a plan containing the charge axis, $\mathcal{P}_x$, with eigenvalues $\epsilon = +, -$.

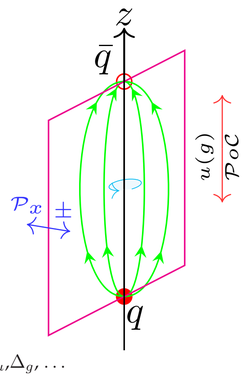

The possible quantum numbers are: Σ_g^+, Σ_g^-, Σ_u^+,Σ_u^-,Π_g,Π_u, Δ_u,Δ_g, ...

4 Anisotropic Wilson action

In this work, we use the Wilson action discretized on anisotropic lattices, which is obtained as:

$$S_{\text{Wilson}} = \beta \left(\frac{1}{\xi} \sum_{x,s>s'} W_{s,s'} + \xi \sum_{x,s} W_{s,t} \right), \tag{3}$$

where $\beta = 6/g^2$ is the inverse coupling and ξ is the bare anisotropic factor defined as the ratio of spatial lattice spacing to temporal lattice spacing (a_s/a_t). Furthermore, $W_c = \sum_c \frac{1}{3}\mathrm{Re\,Tr}(1 - P_c)$, , where s, s' run over spatial links in different positive directions, $P_{s,s'}$ denotes the spatial plaquette, and $P_{s,t}$ the spatial-temporal plaquettes.
Using the anisotropic action allows for a finer lattice in the temporal direction and a coarser lattice spacing in the spatial direction. As a result, we have more data points in the effective mass plot and can study larger distances. Using the action above, we have generated ensembles listed in Table 1 below.

Ensemble	N_c	β	ξ	ξ_r	Volume	$a_t\sqrt{\sigma}$	$a_s\sqrt{\sigma}$
$W_{3,2}$	3	5.90	2.00	2.1737(4)	$24^3 \times 48$	0.1403(8)	0.3049(17)
$W_{3,4}$	3	5.70	4.00	4.5363(8)	$24^3 \times 96$	0.0887(4)	0.4023(16)
$W_{4,2}$	4	10.70	2.00	2.0958(2)	$24^3 \times 48$	0.1680(2)	0.3521(5)
$W_{4,4}$	4	10.40	4.00	4.2940(5)	$24^3 \times 96$	0.1018(3)	0.4372(12)
$W_{5,2}$	5	17.20	2.00	2.0596(1)	$24^3 \times 48$	0.1451(3)	0.2988(5)
$W_{5,4}$	5	16.50	4.00	4.1853(3)	$24^3 \times 96$	0.1025(0)	0.4288(1)
$W_{6,4}$	6	24.00	4.00	4.1274(2)	$24^3 \times 96$	0.0996(0)	0.4113(2)

Table 1: Details for the ensembles generated using the anisotropic Wilson action. ξ_r is the normalized anisotropic factor, and each ensemble includes 1000 configurations. All ensembles have been smeared 100 times using multihit in the temporal direction and APE smearing ($\alpha = 0.3, n_s = 20$) in the spatial directions.

5 Obtaining the Excitations

To compute the spectra of the flux tube, we first calculate the Wilson correlation matrix $\mathcal{C}(r,t)$. The entry $\mathcal{C}_{i,j}(r,t)$ of the Wilson correlation matrix is the expectation value of spatial-temporal closed loops (Fig. 1), where the spatial sides are replaced with operators O_i and O_j that have identical symmetry to the flux tube of interest.

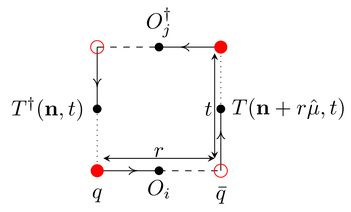

Fig. 1: A closed loop corresponds to the entry $\mathcal{C}_{i,j}(r,t)$ of the Wilson correlation matrix.

For example, O_i and O_j can be constructed using the staples shown in Figs. 2 to 5.
Next, we find the generalized eigenvalues λ of the Wilson correlation matrix:

$$\mathcal{C}(r,t)\vec{v}_n = \lambda_n(r,t)\mathcal{C}(r,t_0)\vec{v}_n, \tag{4}$$

where we set $t_0 = 0$. Consequently, we obtain a set of time-dependent eigenvalues $\lambda_n(t)$ for each r. We then order the eigenvalues and plot the effective mass defined as:

$$E_i(r) = \ln \frac{\lambda_i(r,t)}{\lambda_i(r,t+1)}. \tag{5}$$

The plateau in the effective mass plot corresponds to the energy $E_i(r)$.

6 Topological Charge

The topological charge is defined as

$$Q = \frac{1}{32\pi^2} \int d^4x\, \epsilon_{\mu\nu\rho\sigma}\, \mathrm{Tr}\left[G_{\mu\nu}(x) G_{\rho\sigma}(x)\right]. \tag{6}$$

where $G_{\mu\nu}$ is the field strength tensor of the gauge field. In simulations of large-N_c gauge fields, it is crucial to track the topological charge to ensure the ergodicity of the Monte Carlo process. As N_c increases, the topological charge tends to freeze. In Fig. 8, we show the time progression of the topological charge for the largest $N_c = 6$, confirming that in our simulation, the topological charge is not frozen, and thus the simulation is ergodic.

RESULTS

7 Operators

In this work, we use the operators, already used in Ref. [4] to study $SU(3)$ spectra. Here are the shapes of the stables used to build up the operators for different flux tube symmetries.

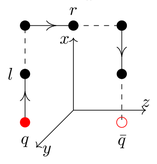

Fig. 2: These staples used for Σ_g^+, Π_u, and Δ_g flux tube.

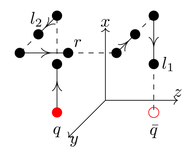

Fig. 3: These staple used for Σ_g^- flux tube.

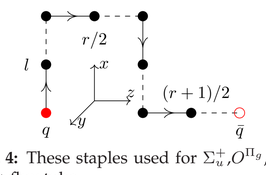

Fig. 4: These staples used for Σ_u^+,O^{Π_g},and O^{Δ_u} flux tube.

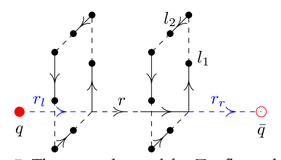

Fig. 5: These staple used for Σ_u^- flux tube.

8 Spectra of different flux tube symmetries

In this section, we show the spectra of the largest $N_c = 6$ for eight symmetries of the flux tube.

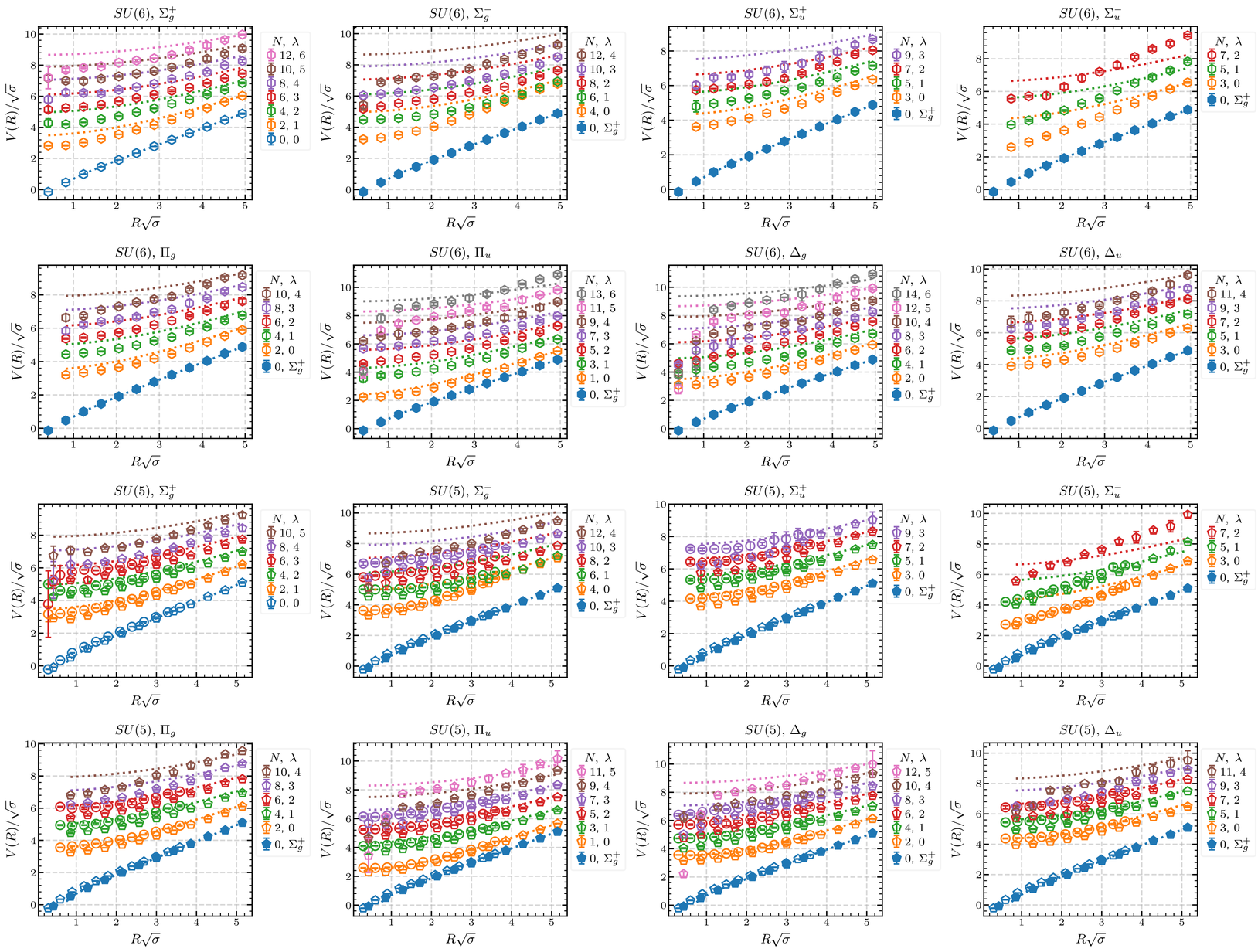

Fig. 6: Polygonal shapes in each figure show the simulation with $\xi = 4$, while circle markers indicate $\xi = 2$. N is the quantum number as defined in Eq. 2, and λ is the excitation number.

9 States With Axion

Considering the spectra shown in Fig. 6, we observe that the Σ_u^- flux tube and the ground state of Σ_g^- are not compatible with the Nambu-Goto model. In the following figures, we demonstrate the presence of axions in these open flux tubes with the same mass as the axions obtained from the closed flux tube spectra.

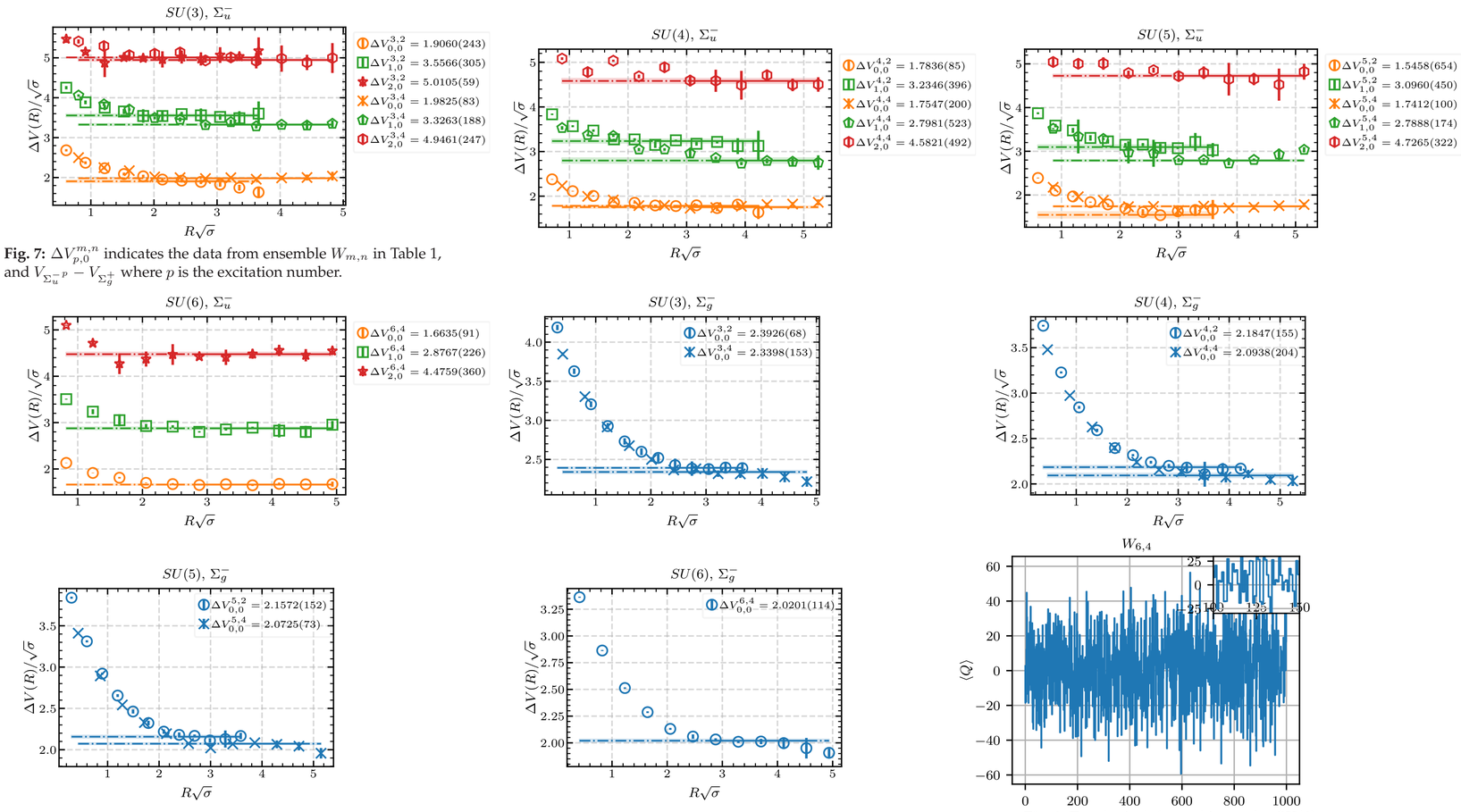

Fig. 7: $\Delta V_{p,0}^{m,n}$ indicates the data from ensemble $W_{m,n}$ in Table 1, and $V_{\Sigma_u^{-p}} - V_{\Sigma_g^+}$ where p is the excitation number.

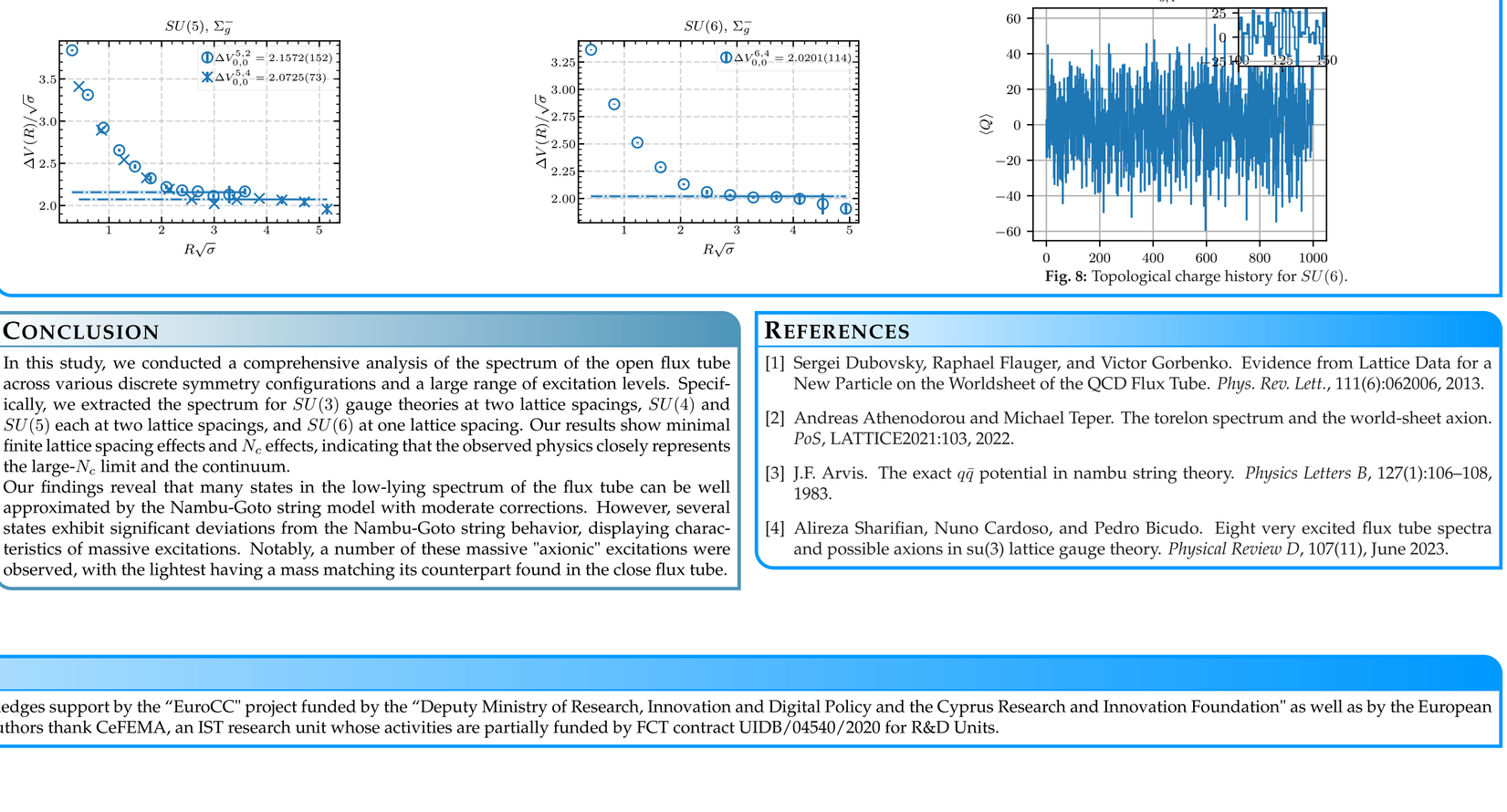

Fig. 8: Topological charge history for $SU(6)$.

CONCLUSION

In this study, we conducted a comprehensive analysis of the spectrum of the open flux tube across various discrete symmetry configurations and a large range of excitation levels. Specifically, we extracted the spectrum for $SU(3)$ gauge theories at two lattice spacings, $SU(4)$ and $SU(5)$ each at two lattice spacings, and $SU(6)$ at one lattice spacing. Our results show minimal finite lattice spacing effects and N_c effects, indicating that the observed physics closely represents the large-N_c limit and the continuum.
Our findings reveal that many states in the low-lying spectrum of the flux tube can be well approximated by the Nambu-Goto string model with moderate corrections. However, several states exhibit significant deviations from the Nambu-Goto string behavior, displaying characteristics of massive excitations. Notably, a number of these massive "axionic" excitations were observed, with the lightest having a mass matching its counterpart found in the close flux tube.

REFERENCES

[1] Sergei Dubovsky, Raphael Flauger, and Victor Gorbenko. Evidence from Lattice Data for a New Particle on the Worldsheet of the QCD Flux Tube. *Phys. Rev. Lett.*, 111(6):062006, 2013.

[2] Andreas Athenodorou and Michael Teper. The torelon spectrum and the world-sheet axion. *PoS*, LATTICE2021:103, 2022.

[3] J.F. Arvis. The exact $q\bar{q}$ potential in nambu string theory. *Physics Letters B*, 127(1):106–108, 1983.

[4] Alireza Sharifian, Nuno Cardoso, and Pedro Bicudo. Eight very excited flux tube spectra and possible axions in su(3) lattice gauge theory. *Physical Review D*, 107(11), June 2023.

ACKNOWLEDGMENT

AS was supported by CEFEMA UIDB/04540/2020 Post-Doctoral Research Fellowship. AA acknowledges support by the "EuroCC" project funded by the "Deputy Ministry of Research, Innovation and Digital Policy and the Cyprus Research and Innovation Foundation" as well as by the European High-Performance Computing Joint Undertaking (JU) under grant agreement No 101101903. The authors thank CeFEMA, an IST research unit whose activities are partially funded by FCT contract UIDB/04540/2020 for R&D Units.